Low-energy-electron transmission through epitaxial films: Cu(001) on Ni(001)

Hiroshi Iwasaki,* B. T. Jonker,† and Robert L. Park
Department of Physics and Astronomy, University of Maryland, College Park, Maryland 20742
(Received 26 November 1984)

Low-energy- (<10 eV) electron transmission spectra were measured for electrons normally incident on epitaxial Cu(001) films on a Ni(001) substrate for coverages of zero to several tens of monolayers (ML). Electron transmission spectra exhibited characteristic quantum size-effect (QSE) features for discrete coverages. The QSE features in the energy gap of the substrate and its vicinity are stronger than those in the allowed energy band due to strong Bragg reflection of electrons at the film substrate interface. From the steplike increases in the transmission current, we obtain values for the upper band-gap edges (X_1 point) for the clean Ni(001) substrate and a thick Cu(001) overlayer of 9.5 and 7.3 eV above the Fermi level, respectively. A one-dimensional theory of electron transmission for over-layered crystals based on low-energy electron diffraction theory is presented, which incorporates the band structures of the materials in the [001] direction. The calculated transmission spectra are sensitive to the lattice spacing as well as the thickness of the film. With the use of the bulk values of lattice spacings for the film and the substrate, excellent agreement was obtained between the experimental and calculated results for coverages greater than 7 ML, but slight systematic differences were observed for 3 to 6 ML coverages. This suggests that the film is pseudomorphic up to 6 ML, after which the entire film rearranges itself to assume the bulk Cu structure.

I. INTRODUCTION

Electron-transmission (or reflection) measurements have been employed by many investigators to study surfaces and overlayers of solids. Andersson and Kasemo[1] have investigated electron reflectivities from disordered overlayers of alkaline adsorbates on nickel surfaces and have derived the overlayer-substrate distance. Thomas[2] clearly observed quantum size effects in electron transmission through epitaxial metal films on a single-crystal substrate and obtained values for the inner potential and electron mean-free-path lengths of the film. Jonker *et al.*[3,4] have recently shown that the quantum size effect (QSE) can be used to investigate the film/substrate interface itself. Quantum size oscillations have been observed in electron tunneling in thin metal-oxide-semiconductor (MOS) structures,[5] too.

Jaklevic and Davis have reported that critical points in the energy bands produce characteristic structure in the low-energy-electron reflectance spectra, and have used this effect to investigate epitaxial metal film growth.[6] Bader *et al.* have reported similar studies for condensed gas films.[7]

To elucidate the effect of film and substrate band structure on the quantum size oscillations observed for epitaxial film growth,[2–4,8] we have chosen an epitaxial system in which both film and substrate have a band gap in the energy range of interest: Cu/Ni(001). The epitaxial system of Cu on Ni(001) is known to produce smooth films of copper oriented to the (001) surface.[9] According to the Auger electron spectroscopy (AES) and electron microscopy studies of Chambers and Jackson,[9] the Cu films tend to grow in a layer-by-layer fashion at room temperature and are strained compressively to be coherent with the substrate (pseudomorphic) up to a thickness of 8 Å. Above this thickness the elastic strain decreases with the introduction of misfit dislocations, but more rapidly than theory predicts[9] (13–14 Å).

A free-electron rectangular-well–type potential model has previously been used to qualitatively interpret the QSE data.[2,3,8] Although such a model provides a remarkably successful description of QSE for some systems[3,4] and illustrates the effect of various film and interface parameters, it fails to quantitatively account for the transmission spectra of Cu(001) films on a Ni(001) substrate.

In this paper we present a simple theory of low-energy-electron transmission for an overlayered crystal which utilizes low-energy-electron diffraction (LEED) theory[10] to include the effect of the band structures of the film and substrate. At the low electron energies of interest in such measurements (below the nonspecular beam emergence threshold) a one-dimensional model is valid and calculations are greatly simplified. We compare the results of these calculations with the experimentally measured electron transmission spectra for epitaxially grown Cu films on a Ni(001) substrate for coverages of zero to several tens of monolayers (ML), and show that the experimental results are well reproduced by calculations which incorporate the band structures of Cu and Ni along the (001) direction in the energy range of interest (0–10 eV relative to the vacuum level). Features in the experimental transmission spectra associated with band gaps in the film and substrate are readily accounted for by using the accepted bulk parameters. QSE features in the energy gap of the substrate and its vicinity are found to be stronger than those in the allowed energy band due to strong Bragg reflection of electrons at the film/substrate interface. We obtain values for the upper band-gap edges (X_1 point) of Ni and Cu (001) of 9.5 and 7.3 eV relative to the Fermi

energy from the steplike increases in the transmission current for the clean Ni substrate and thick Cu(001) films, respectively. Comparison with the model calculations suggests that the Cu films are pseudomorphic up to 6 ML, while thicker Cu films assume the bulk structure. These results show that low-energy-electron transmission spectroscopy is useful to monitor the epitaxial growth process and to study structural and electronic properties of the overlayered crystals.

II. EXPERIMENTAL

A. Experimental method

The experiments were conducted in a stainless-steel, sputter-ion and titanium-sublimation pumped ultrahigh-vacuum system with a base pressure of less than 1×10^{-10} Torr. The system is equipped with a high-precision sample manipulator, high-purity O_2 and Ar gas handling facilities, a commercial 4-grid LEED-Auger optics, an ion-bombardment gun, a field-emission gun, and a quartz-crystal monitored evaporation oven. Sample surface structure and cleanliness were checked with low-energy-electron diffraction and Auger electron spectroscopy (AES). The sample was mounted on a heater which permitted indirect resistive heating, and the temperature measured by a chromel-alumel thermocouple attached to the side of the sample. The Ni surface was cleaned in a conventional manner by Ar^+-ion sputtering and annealing followed by heating at 350 °C in an oxygen pressure of 10^{-8} Torr and flashing to 550 °C to desorb the oxygen. The only surface contaminant present after this treatment was a small amount of carbon which was estimated to be less than 3% of a monolayer and could not be reduced further.

Copper was evaporated onto the clean, room-temperature Ni(001) substrate at normal incidence from a well out-gassed tungsten basket at a rate of approximately 0.2 ML per second. The background pressure typically rose no higher than 5×10^{-10} Torr during evaporation. A quartz-crystal microbalance mounted next to the substrate approximately 20 cm from the tungsten basket was used to monitor the evaporation. The resultant copper films exhibited excellent long-range order as demonstrated by the sharp LEED pattern they produced, and AES spectra of the film surfaces showed no detectable contamination.

Retarding potential measurements of the sample current versus incident electron energy were made at normal incidence using either the electron gun of the LEED optics, operated at 250 V with a retarding potential applied to the sample, or with a second electron gun operated near ground potential with the sample at ground. Derivatives of the sample current were obtained by the potential modulation technique using a 0.3-eV (peak-to-peak) modulation voltage; the energy of a peak in a spectrum could be determined to an accuracy of 0.1 eV. Normal incidence was established using the LEED optics so that the (01) beams disappeared simultaneously with decreasing electron energy and the specular beam was reflected directly back down the electron gun. The reflected current from the sample was also measured by the LEED optics.

B. Experimental results

Experimental plots of the sample current and its second derivative vs normally incident electron energy are shown in Fig. 1 for the clean Ni(001) surface and a thicker (~25 ML) Cu(001) epitaxial layer. As the electron energy is increased, the electrons can surmount the work-function barrier and are detected as a sample current; the turn on at the work-function threshold produces the steplike increase in each sample current spectrum. An abrupt steplike increase in the sample current produces a negative and positive excursion in the second-derivative spectrum I_s''. The zero of energy in Fig. 1 is referenced to the Fermi level by using a value of 4.80 ± 0.05 eV for the work function of Cu(001), as measured here by the field emission retarding potential technique. The sample current for Ni(001) was very sensitive to the presence of oxygen on the surface; oxygen adsorption from the residual gas changes the first plateau (6–9 eV) to a dip in the I_s curve.

There are features of negative and positive excursion in the second-derivative spectra for both the clean Ni(001) surface and for the thick Cu film (~25 ML) above the work-function thresholds (Fig. 1). These features correspond to the upper edges of the first band gap for Ni(001) and Cu(001) (X_1 points). The second-derivative transmission spectra enable one to determine these energies precisely as the inflexion point between excursions. These values are 9.5 and 7.3 eV for Ni(001) and Cu(001), respectively, measured from the Fermi level.

Experimental plots of the second derivative of the sample current versus normally incident electron energy are shown in Fig. 2 for the clean, 1- and 15-ML Cu-covered

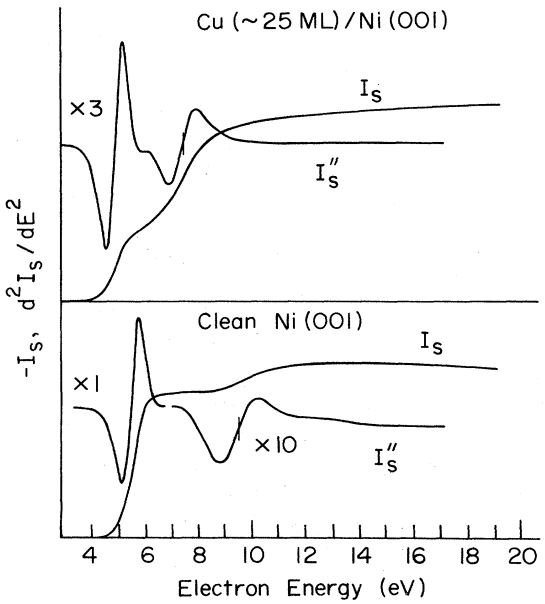

FIG. 1. Experimental plots of the sample current I_s and its second derivative I_s'' as a function of normally incident electron energy for the clean Ni(001) surface (bottom) and a 25-monolayer-thick Cu(001) epitaxial film (top). The zero of energy is at the Fermi level. The prominent feature above the work function threshold in the I_s'' spectra corresponds to the upper edge of the first band gap (X_1 point).

Ni(001) surfaces. As Cu is evaporated onto the surface, the threshold shifts to lower energy by 0.6 ± 0.1 eV, representing a decrease in work function. Remarkably, the work-function decrease is completed for a single monolayer within the experimental accuracy. The zero of energy is chosen to be at the Fermi level. Figure 3 shows experimental spectra for Cu coverages of 2 to 14 ML in 1-ML increments. Nearly identical results are obtained by measuring either the reflected current, which includes both elastic and inelastic components, or the sample current.

By 1-ML Cu coverage, the negative excursion at 9 eV obtained for the clean Ni surface is weakened and the feature becomes a single dominant peak shifted to lower incident energy (Fig. 2). The origin of the small features seen at lower energy (6—7.3 eV) in several spectra is not clear at present. For increasing Cu coverages, one observes the following in Figs. 2 and 3:

(i) the dominant peak shifts to lower energy,

(ii) additional smaller peaks develop on the high-energy side of this leading peak due to quantum size effects,[2,3]

(iii) the intensities of peaks which lie below the upper edge of the Ni(001) band gap at 9.5 eV, $\epsilon_{g\,\max}$(Ni), are much stronger than the peaks well above $\epsilon_{g\,\max}$(Ni),

(iv) the lowest energy peak is always dominant and it moves steadily down to the upper edge of the first band gap of the Cu(001) film (7.3 eV),

(v) for higher coverages, the negative excursion of the lowest energy peak increases and finally changes to a full negative and positive excursion-type feature corresponding to an abrupt, steplike increase in the sample current.

These results show that the QSE features for the present Cu/Ni(001) system are strongly affected by the band structures of the film and the substrate. Band-structure effects were not evident in previous results, taken on a system that had no band edges in the region of interest. Therefore, we present a theory of electron transmission for overlayered crystals based on LEED theory which quantitatively incorporates the band structures of the film and the substrate in the following section.

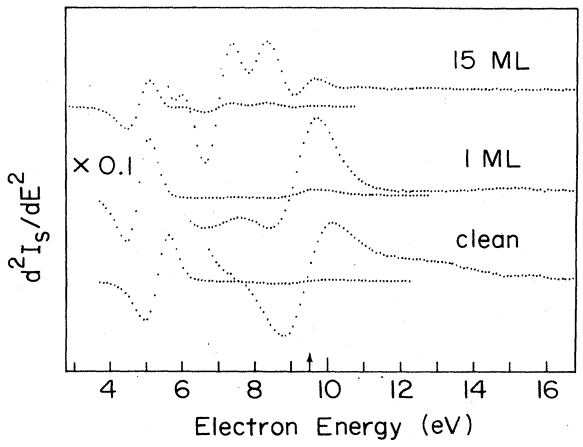

FIG. 2. Experimental plots of the second derivative of the sample current vs electron energy (referred to the Fermi level) for clean Ni(001) surface and Cu coverages of 1 and 15 monolayers. The energy corresponding to the X_1 point of Ni is marked by an arrow.

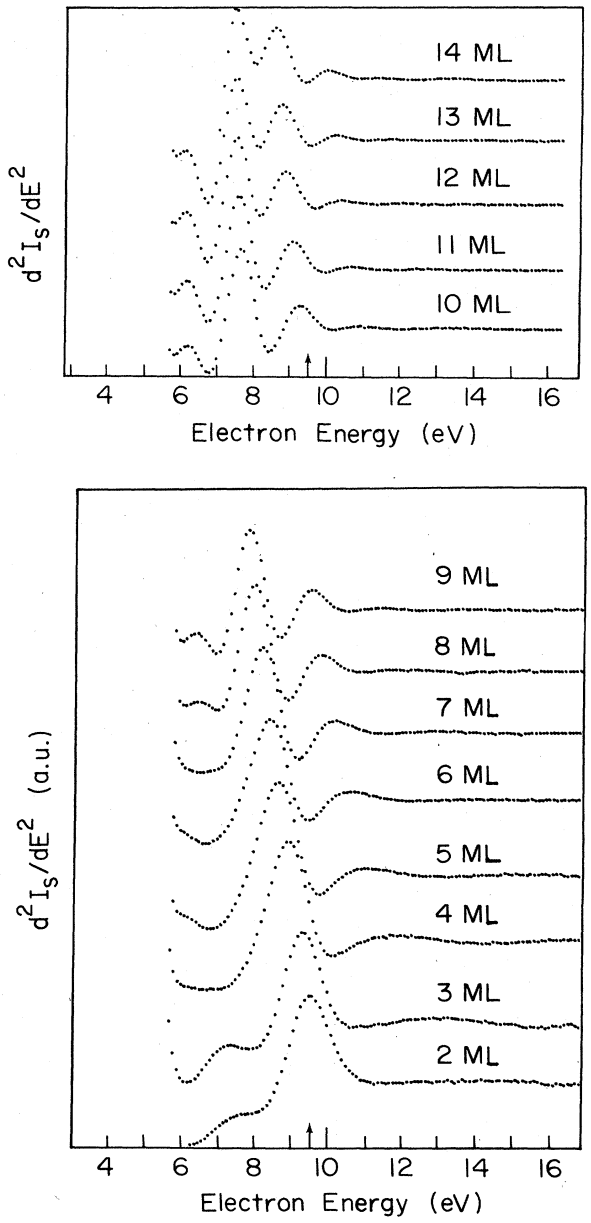

FIG. 3. Expanded experimental electron transmission spectra for 2- to 14-ML Cu-covered Ni(001) surfaces. The energy corresponding to the X_1 point of Ni is marked by an arrow.

Figure 4 shows the elastic component of the reflected current from a Cu-covered Ni sample as a function of the incident energy for normal incidence [Fig. 4(a)] and slightly off-normal incidence [Fig. 4(b)]; the specularly reflected beam is excluded from the collected current in Fig. 4(a), since it returns down the electron gun axis and is not detected, and it is included in Fig. 4(b). Both curves were recorded at the same sensitivity on a lock-in amplifier. The quantum size features clearly seen in Fig. 4(b) are totally absent from Fig. 4(a). Thus, the quantum size

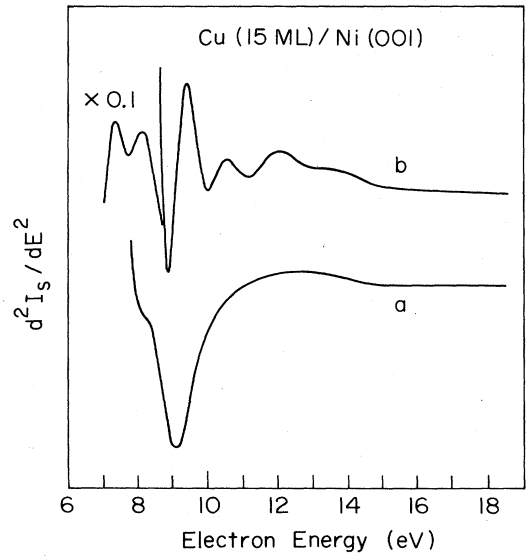

FIG. 4. Experimental plots of second derivative of the elastically reflected current vs electron energy (referred to the Fermi level) for a 15-ML Cu-covered Ni(001) surface at (a) normal incidence and (b) off-normal incidence. The QSE features present in (b) are absent from (a) because at exact normal incidence the specular beam returns down the axis of the electron gun and is not collected.

features are seen in the specularly reflected electron beam but not in the angular-integrated diffusely scattered one.

III. THEORY

A. Formulation

For very low energies (≤ 10 eV), the electron wavelength exceeds the nearest-neighbor spacings along the interface, so that only scattering into the forward or specularly reflected beam occurs. This is generally the case for a metal/metal epitaxial system for electron energies below about 10 eV. In this case, a one-dimensional model of electron transmission is valid, and may be reasonably applied to the problem we address here. The fact that among the elastically scattered electrons only the specular beam contains the quantum size feature (Fig. 4) shows that the electrons contributing to this effect are, in fact, specularly scattered at the interfaces and justifies the one-dimensional theory of QSE. We base the following model of electron transmission through an epitaxial film on a crystal substrate on Pendry's one-dimensional multiple-scattering LEED theory.[10]

We adopt the model illustrated in Fig. 5. The film is assumed to consist of a regular array of m layers of scattering potentials on a semi-infinite substrate. Each scatterer is the analog of a plane layer of ion cores. A uniform background potential U_1 or U_2 (muffin-tin potentials) exists between the scattering centers for the film and the substrate (subscripts 1 and 2 hereafter refer to film and substrate, respectively). U_1 and U_2 may have imaginary components to include absorption. The surface and film/substrate interface planes are located half a

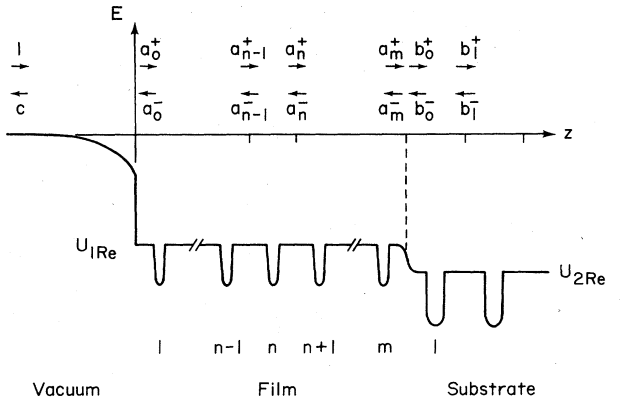

FIG. 5. One-dimensional potential model of a multi-overlayered crystal. Coefficients of forward and backward traveling waves far from the surface and between scatterers are also shown. The zero of energy is at the vacuum level of the film.

lattice-plane separation from the adjacent lattice planes. At the surface and the film/substrate interface, the potentials are appropriately connected as shown later.

In the vacuum far from the sample, the potential is constant and chosen to be zero. There plane-wave solutions of the Schrödinger equation exist of the form

$$\psi=\exp(ik_0z)+C\exp(-ik_0z)\ ,\qquad \frac{\hbar^2}{2m}k_0^2=\epsilon \tag{1}$$

where m is the free electron mass and C is the amplitude of the reflected wave. Normalizing the incident wave gives the following expression for the transmitted intensity T:

$$T=1-|C|^2\ . \tag{2}$$

Inside the film, the wave function in the region of constant potential between the nth and $(n+1)$th scatterers may be written

$$\psi_{1n}=a_n^+\exp[ik_1(z-nd_1)]+a_n^-\exp[-ik_1(z-nd_1)]\ ,\qquad \frac{\hbar^2}{2m}k_1^2=\epsilon-U_1\ , \tag{3}$$

where d_1 is the interlayer spacing of the film.

In a similar manner, the wave function in the constant potential region immediately inside the substrate may be written

$$\psi_{20}=b_0^+\exp[ik_2(z-md_1)]+b_0^-\exp[-ik_2(z-md_1)]\ ,\qquad \frac{\hbar^2}{2m}k_2^2=\epsilon-U_2\ , \tag{4}$$

where m is the number of overlayer planes or scatterers.

The scattering potentials can be characterized by transmission and reflection coefficients t_i and r_i $(i=1,2)$ which give the probability amplitude that the electron will be transmitted through or reflected from the scatterer; they depend on the incident wave vector k_i in a manner determined by the detailed features of the scattering potentials $V_i(z)$. As $V_i(-z)=V_i(z)$ for Ni and Cu in the

[001] direction, t_i and r_i are the same for electrons incident from the left and from the right on $V_i(z)$. We choose t_i and r_i so that they reproduce calculated bulk band structures as shown later.

We assume that no flux is lost by absorption within the scatterers. Then electron conservation requires that the probability of transmission plus the probability of reflection be unity:

$$|t_i|^2+|r_i|^2=1 . \tag{5}$$

We choose t to be a complex number rather than a real number as Pendry did[10] and write it in terms of its magnitude and phase:

$$t=|t|\exp(i\delta) . \tag{6}$$

It can be shown that rt^* is pure imaginary (see Ashcroft and Mermin[11]). Thus r must have the form

$$r=\pm|r|\exp(i\delta) . \tag{7}$$

We now derive equations for the coefficients a_n^+ and a_n^- of the wave function in the film in terms of t_1 and r_1. There are two contributions to a_n^+, the amplitude of the forward traveling wave in the constant potential region between the nth and $(n+1)$th scatterers: transmission of the forward traveling wave $a_{n-1}^+\exp\{ik_1[z-(n-1)d_1]\}$ through the nth scatterer, and reflection of the backward traveling wave $a_n^-\exp[-ik_1(z-nd_1)]$ at the nth scatterer. After taking into account a phase factor we immediately have

$$a_n^+=(r_1a_n^-+t_1a_{n-1}^+)\alpha_1^{-1} , \tag{8}$$

where

$$\alpha_1=\exp(-ik_1d_1) .$$

In a similar way, a_{n-1}^- can be written

$$a_{n-1}^-=(r_1a_{n-1}^++t_1a_n^-)\alpha_1^{-1} . \tag{9}$$

For the substrate there exist equations similar to Eqs. (8) and (9),

$$b_j^+=(r_2b_j^-+t_2b_{j-1}^+)\alpha_2^{-1} , \tag{10}$$

$$b_{j-1}^-=(r_2b_{j-1}^++t_2b_j^-)\alpha_2^{-1} , \tag{11}$$

where

$$\alpha_2=\exp(-ik_2d_2) .$$

Since the substrate is assumed to be infinite, we may apply the Bloch condition to the substrate wave functions. This condition may be written

$$b_j^+=\beta b_{j-1}^+ , \tag{12}$$

$$b_j^-=\beta b_{j-1}^- , \tag{13}$$

where $\beta=\exp(iKd_2)$ and K is the Bloch wave vector. Using this condition, we may rewrite Eqs. (10) and (11) as follows (subscript 2 is omitted for convenience):

$$(t-\beta\alpha)b_j^++\beta rb_j^-=0 , \tag{14}$$

$$rb_j^++(\beta t-\alpha)b_j^-=0 . \tag{15}$$

For the above equations to have a solution, β must be given by

$$\beta=\frac{\gamma^2+\alpha^2\pm[(\gamma^2+\alpha^2)^2-4\alpha^2t^2]^{1/2}}{2\alpha t} , \tag{16}$$

where we have used Eqs. (6) and (7) and set $\gamma=\exp(i\delta)$. There are two solutions (Bloch waves). The ratio of b_j^+ to b_j^- is

$$b_j^+/b_j^-=-(\beta t-\alpha)/r . \tag{17}$$

The probability density P_j of electrons at the jth site of the substrate is obtained from Eqs. (4), (12), and (13),

$$\begin{aligned}P_j&=|b_j^++b_j^-|^2\\&=|\beta|^{2j}|b_0^++b_0^-|^2\\&=\exp(-2K_{\mathrm{Im}}jd_2)|b_0^++b_0^-|^2 ,\end{aligned} \tag{18}$$

where K_{Im} is the imaginary part of the Bloch wave vector K. Even in the absence of absorption K_{Im} is nonzero within the band gaps. Thus a physically realistic solution demands that we choose β as given by Eq. (16) so that K_{Im} is positive, hence choosing the mode which decreases further into the substrate. When U_2 is real (absence of inelastic or incoherent scattering), K_{Im} is zero in the allowed bands. In this case we choose the solution which carries net flux into the crystal. This is realized when $|b_j^+/b_j^-|^2$ is greater than 1.

For an electron of low kinetic energy (<40 eV), scattering by the surface and the film/substrate interface depends strongly on the shape of the potential assumed to represent the interface. A square potential step is a poor approximation to the true shape of the potential at the interfaces, since the so-called optical or inner potential cannot die away on a scale much less than the Thomas-Fermi screening length L (~0.5 Å for Ni and Cu).[10] Classically, the surface barrier must include the effect of an image potential, and at large distances the classical image model should be an adequate representation of the potential above a metal surface. The actual form of the potential in the near surface region, unfortunately, is not known. The results of Dietz, MacRae, and Campbell,[12] however, suggest that the image potential very near the surface is saturated and significantly more abrupt than the classical image model. Even less is known about the form of the potential at the metal/metal interface. The change in potential between the film and substrate must clearly occur over some finite distance. We thus choose potential barriers at the film surface and the film/substrate interface to be of the general form

$$U(z)=U_a+U_b/[1+\exp(z/L)] . \tag{19}$$

We consider two different surface potential barriers, $U_{V1}(z)$ and $U_{V2}(z)$. $U_{V1}(z)$ varies smoothly through and on either side of the surface plane and is given by

$$U_{V1}(z)=U(z) , \tag{20}$$

where $U_a=-U_b=U_{1\mathrm{Re}}$ and $U_{1\mathrm{Re}}$ is the real part of U_1. The center of the barrier, $z=0$, is chosen to lie in a plane tangential to the muffin tins of the last layer of film atoms (see Fig. 5). The second surface barrier, $U_{V2}(z)$, ex-

hibits an abrupt step at the surface ($z=0$) as shown in Fig. 5, and is given by

$$U_{V2}(z)=\begin{cases}U(z) & \text{for } z<0\ ,\\ U_1 & \text{for } z\geq 0\ ,\end{cases} \tag{21}$$

where $U_a=-U_b$ is not necessarily equal to $U_{1\,\mathrm{Re}}$. According to Pendry,[10] the imaginary part of the optical potential $U_{1\,\mathrm{Im}}$ must decay into the vacuum more quickly than $U_{1\,\mathrm{Re}}$. In the present calculation $U_{1\,\mathrm{Im}}$ is simply chosen to be zero for $z<0$.

The potential at the interface between the film and the substrate, $U_{\mathrm{fs}}(z)$, is chosen to be

$$\begin{aligned}&U_{\mathrm{fs}}(z)=U(z-md_1)\ ,\\ &U_a=U_{2\,\mathrm{Re}},\quad U_b=U_{1\,\mathrm{Re}}-U_{2\,\mathrm{Re}}\ ,\end{aligned} \tag{22}$$

where $U_{2\,\mathrm{Re}}$ is the real part of U_2. We assume that the imaginary parts of the constant potentials change abruptly from $U_{1\,\mathrm{Im}}$ to $U_{2\,\mathrm{Im}}$ at the film/substrate interface.

The potential barriers $U_{V1}(z)$ and $U_{\mathrm{fs}}(z)$ at the vacuum/film and the film/substrate interfaces can be thought of as additional layers with different scattering properties placed at the interfaces if $L\ll d_1$ and d_2. We now define r_V^+ and r_V^- (t_V^+ and t_V^-) as reflectivities (transmissivities) of the surface potential barrier $U_{V1}(z)$ for electrons incident on the barrier from the vacuum side and from the film side, respectively. Similarly, we define reflectivities (transmissivities) of the film/substrate interface potential $U_{\mathrm{fs}}(z)$ as r_{fs}^+ and r_{fs}^- (t_{fs}^+ and t_{fs}^-) for electrons incident on the potential from left to right and from right to left, respectively. These are given in the Appendix.

Following the same procedure used to derive Eqs. (8)—(11), we obtain the two relations at the surface,

$$C=r_V^+ +t_V^- a_0^-\ , \tag{23}$$

$$a_0^+ =t_V^+ +r_V^- a_0^-\ . \tag{24}$$

Similarly, at the film/substrate interface, we obtain

$$a_m^- =r_{\mathrm{fs}}^+ a_m^+ +t_{\mathrm{fs}}^- b_0^-\ , \tag{25}$$

$$b_0^+ =t_{\mathrm{fs}}^+ a_m^+ +r_{\mathrm{fs}}^- b_0^-\ . \tag{26}$$

For the surface potential barrier $U_{V2}(z)$, we may follow the same procedure outlined above, but with no limitation on the parameter L. Alternatively, we may match the waves outside and inside the film in amplitude and derivative at the surface ($z=0$). The wave function in vacuum is given by

$$\psi=C_1\psi_1(\nu,\mu,y)+C_2\psi_2(\nu,\mu,y)\ , \tag{27}$$

where C_1 and C_2 are the coefficients to be determined, y is a reduced variable of z, and ψ_1 and ψ_2 include independent hypergeometric functions as given in the Appendix together with ν and μ. The matching condition at the surface yields

$$C_1\psi_1(\nu,\mu,0.5)+C_2\psi_2(\nu,\mu,0.5)=a_0^+ +a_0^-\ , \tag{28}$$

$$C_1\psi_1'(\nu,\mu,0.5)+C_2\psi_2'(\nu,\mu,0.5)=ik_1a_0^+ -ik_1a_0^-\ , \tag{29}$$

where the prime denotes first derivative of the function with respect to z.

The asymptotic form of ψ at $z\rightarrow-\infty$ is

$$\begin{aligned}\psi\rightarrow&[C_1A(\nu,\mu)+C_2A(-\nu,\mu)]e^{ikz}\\ &+[C_1A(\nu,-\mu)+C_2A(-\nu,-\mu)]e^{-ikz}\ ,\end{aligned} \tag{30}$$

where $A(\nu,\mu)$ is given in the Appendix. Again, since ψ must be of the form

$$\psi=\exp(ikz)+C\exp(-ikz) \tag{31}$$

as $z\rightarrow-\infty$, we must have

$$C_1A(\nu,\mu)+C_2A(-\nu,\mu)=1\ , \tag{32}$$

$$C_1A(\nu,-\mu)+C_2A(-\nu,-\mu)=C\ . \tag{33}$$

In the case of the surface potential barrier $U_{V1}(z)$, Eqs. (8), (9), (17), and (23)—(26) comprise a set of linear equations for the coefficients C, a_n^+, a_n^- ($n=0,1,2,\ldots,m$), b_0^+, and b_0^-. For the surface potential barrier $U_{V2}(z)$, Eqs. (23) and (24) are replaced by Eqs. (28), (29), (32), and (33) to constitute the set of linear equation for the coefficients C, C_1, C_2, a_n^+, a_n^-, b_0^+, and b_0^-.

Thus the problem of calculating the electron transmission coefficient T [Eq. (2)] is reduced to solving these sets of linear equations.

B. Determination of parameters

The coefficients t_i and r_i describing the scattering properties of the plane layers of the film and substrate are chosen to reproduce the calculated band structures along the (001) direction in the energy region of interest. The energies of band-gap edges are given by the condition[10]

$$\cos^2(kd+\delta)=|t|^2\ . \tag{34}$$

Let $\epsilon_{g\,\mathrm{min(max)}}$ be the lower (upper) edge of the first band gap of Ni or Cu in the (001) direction, i.e., the X_4' (X_1) point. The corresponding free-electron wave vector $k_{g\,\mathrm{min(max)}}$ is given by

$$k_{g\,\mathrm{min(max)}}=[(\epsilon_{g\,\mathrm{min(max)}}-U)/(\hbar^2/2m)]^{1/2}\ . \tag{35}$$

As a first step, we assume t (and thus r) are independent of energy. Then $|t|$ and δ are determined by

$$\cos(k_{g\,\mathrm{min}}d+\delta)/|t|=-1\ , \tag{36}$$

$$\cos(k_{g\,\mathrm{max}}d+\delta)/|t|=-1\ . \tag{37}$$

Solving for δ and $|t|$ gives

$$\delta=\pi-(k_{g\,\mathrm{max}}+k_{g\,\mathrm{min}})d/2\ , \tag{38}$$

$$|t|=-\cos(k_{g\,\mathrm{min}}d+\delta)\ . \tag{39}$$

The reflection coefficient r is obtained from Eqs. (5) and (7).

Thus t and r are completely determined by the lattice constant ($2d$), the muffin-tin zero potential U, and the edges of the first band gap $\epsilon_{g\,\mathrm{min}}(X_4')$ and $\epsilon_{g\,\mathrm{max}}(X_1)$. Since the scattering powers of ion cores are insensitive to their environments, the coefficients t and r obtained using the bulk bands are used for those of the planar lattice scatterer for the film even when layer-spacing is slightly

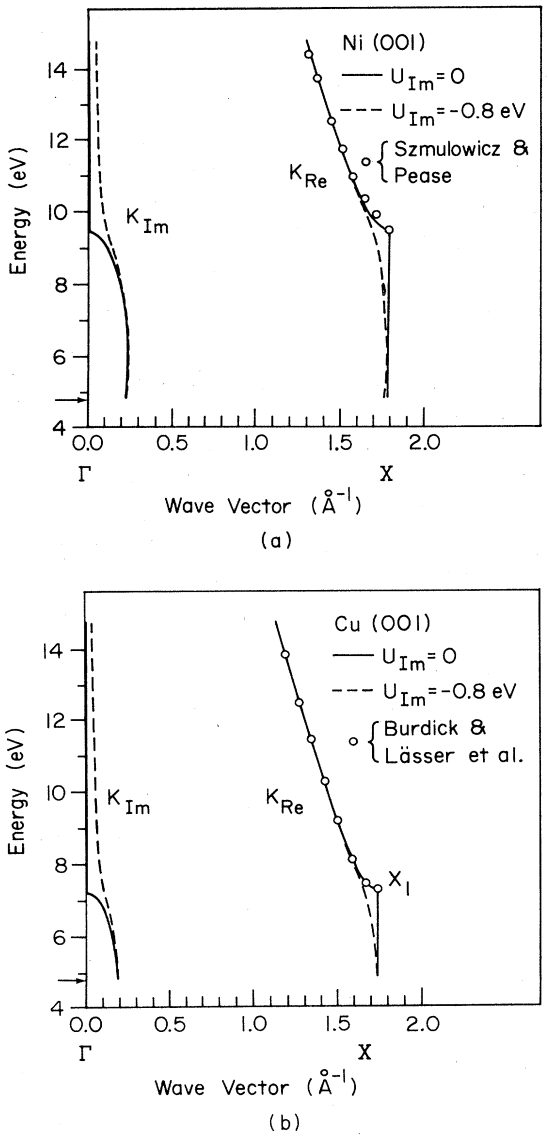

FIG. 6. (a) Dispersion relations obtained for Ni(001) using the parameters stated in the text for $U_{\mathrm{Im}}=0$ eV (no absorption) and $U_{\mathrm{Im}}=-0.8$ eV. The results of the band-structure calculation of Szmulowicz and Pease (Ref. 13) are also shown by open circles for comparison after shifting to fit the X_1 point. The energy corresponding to the work-function threshold of Cu(001) is marked by an arrow. (b) Dispersion relations obtained for Cu(001) in the absence and presence of absorption compared with the band-structure calculations of Burdick (Ref. 14) and Lasser *et al.* (Ref. 16). The energy corresponding to the work-function threshold of Cu(001) is marked by an arrow. In both (a) and (b) the dashed line shows dispersion when absorption is present.

perturbed from the bulk one.

Values of $\epsilon_{g\,\max}$ for Ni and Cu(001) were determined experimentally from the abrupt increase in the transmission current observed when the incident electron energy was increased across the forbidden gap to the allowed bands for the clean Ni substrate and thick Cu films as shown in Sec. II B (see Fig. 1). The values obtained for Ni and Cu (001) are 9.5 and 7.3 eV measured from the Fermi level and are in good agreement with the calculated values of 9.28 eV (Szmulowicz and Pease[13]) and 7.29 eV (Burdick[14]) for Ni and Cu (001), respectively.

The muffin-tin zero potentials $U_{1,2}$ are approximated to be the bottoms of the bands. We use the values of $\epsilon_{g\,\min}$ and U calculated by Szmulowicz and Pease[13] for Ni and those by Burdick[14] for Cu after slightly shifting them so that $\epsilon_{g\,\max}$ coincides with the experimentally obtained values; $\epsilon_{2g\,\min}=2.67$ and $U_2=-8.82$ eV for Ni(001) and $\epsilon_{1g\,\min}=2.04$ and $U_1=-8.96$ eV for Cu(001) relative to the Fermi energy. At low energies the effective potential of the ion cores is weak,[10] and so the muffin-tin zero potential can be identified with the inner potential. By using a value of 4.80 eV for the work function of Cu(001), the muffin-tin zero or inner potential for Cu measured from the vacuum is 13.76 eV. This is in agreement with the value of 13.5 eV obtained by Andersson[15] for Cu(001) using LEED. The result of 11 eV for the inner potential of Cu(111) as determined by earlier QSE studies[3] should be understood as a reduced inner potential seen by a "free electron" in the Cu films. The dispersion curves calculated by different authors agree very closely except for the X_1 point energies—compare, for example, Burdick's[14] result with that of Lässer *et al.*[16] for Cu(001). The lattice constants for bulk Ni and Cu are 3.524 and 3.615 Å, respectively.

Using these parameters, we obtain values for $|t|$, $|r|$, and δ (radian) of 0.920, 0.391, and -0.320 for Ni(001) and 0.946, 0.325, and -0.261 for Cu(001). The imaginary part of U is small for low energies [<15 eV (Ref. 10)] and is chosen to be -0.8 eV for both Ni and Cu. In Figs. 6(a) and 6(b) we show the dispersion relations obtained for Ni and Cu together with the previously reported results in the absence of absorption. The agreement is fairly good and justifies our initial assumption that t and r are independent of energy. Figures 6(a) and 6(b) also show dispersion when absorption ($U_{1,2\,\mathrm{Im}}=-0.8$ eV) is present.

The Thomas-Fermi screening length L is taken to be 0.5 Å for both Ni and Cu.[10] Now only the choice of the surface potential barrier $U_{V1,2}(z)$ and the barrier parameters of U_a ($-U_b$) remain to be determined by fitting the experimental data.

IV. COMPARISON OF CALCULATED AND EXPERIMENTAL RESULTS AND DISCUSSION

In Fig. 7 we compare the experimental spectra with the best-fit calculated results for the clean Ni(001) surface and for Cu coverages of 1 to 15 monolayers. The surface potential $U_{V2}(z)$ [Eq. (21) with $U_a=-U_b=-6.0$ eV] and the $+$ sign in Eq. (7) for r are used in the calculation.

The calculated transmission spectra depend strongly on the choice of sign in Eq. (7) for r, and only the positive sign gives features in agreement with the experimental results. The positive sign means that the scatterers act as net attractive ones.[10] In the nearly-free-electron approximation, $P_j(\epsilon=\epsilon_{g\,\max})$ [Eq. (18)] is proportional to $\cos^2[(\pi/d)jd]$ (or $\sin^2[(\pi/d)jd]$) when the Fourier component of the crystal potential for the wave vector at the X point is negative, i.e., attractive (or positive, i.e., repul-

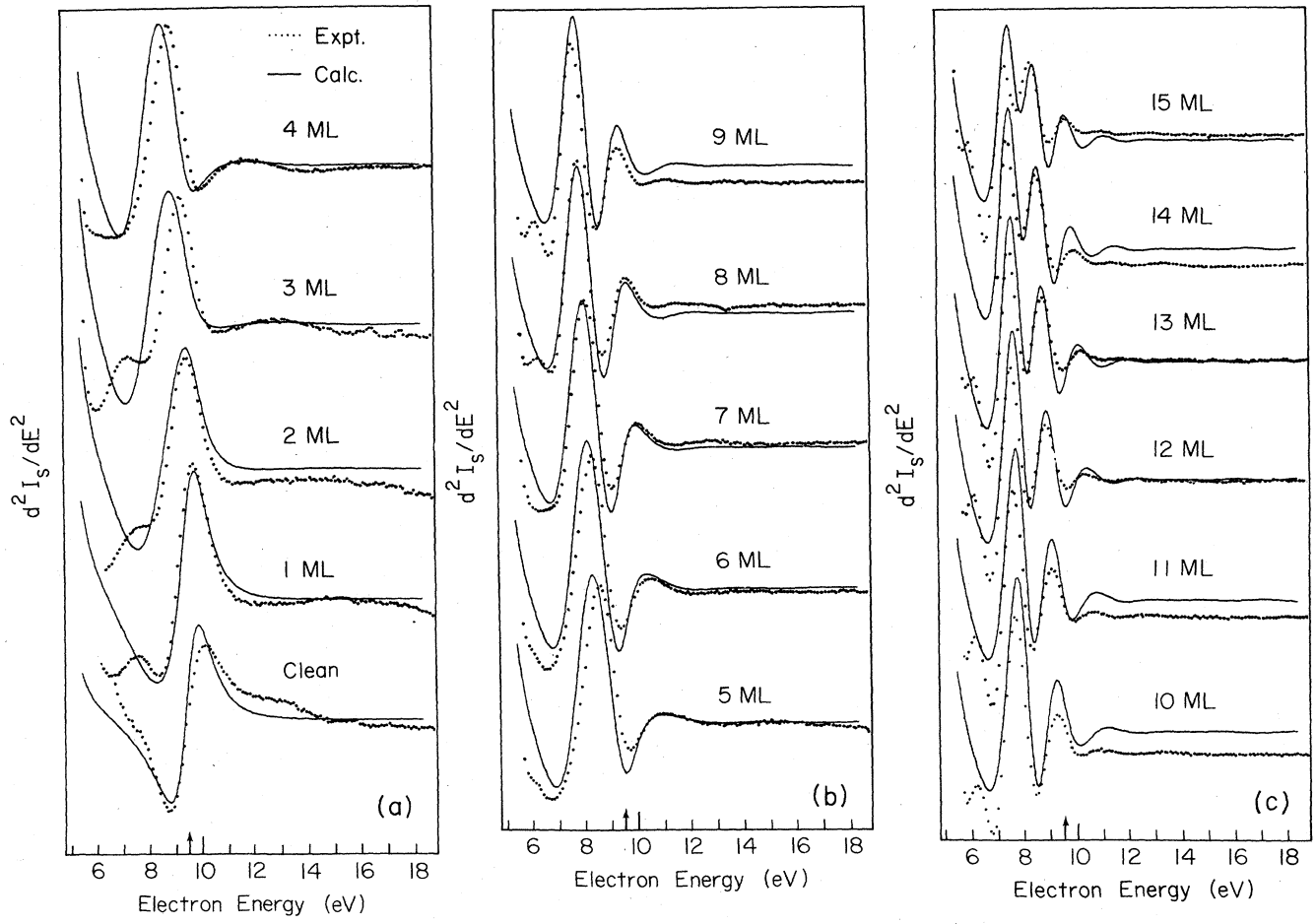

FIG. 7. Experimental electron transmission spectra (•) and calculated curves (——) for clean Ni(001) and for 1- to 15-ML Cu-covered surfaces. The energy corresponding to the X_1 point of Ni is marked by an arrow, and the zero of energy is at the Fermi level. The bulk lattice parameters are used for all the calculated spectra. The 1- and 2-ML spectra are relatively insensitive to changes in the lattice spacing, while the other spectra are reproduced only when the lattice spacing is within ±0.2% of the bulk values. The good agreement for films >7 ML thick shows that the entire film has assumed the bulk Cu structure. The systematic deviations observed for films 3–6 ML thick are attributed to a distortion of the film structure from that of bulk Cu imposed by pseudomorphic growth.

sive). Choosing the + or − sign in Eq. (7) indeed leads to $P_j(\epsilon=\epsilon_{g\,\max})$ of the form $\cos^2[(\pi/d)jd]$ and $\sin^2[(\pi/d)jd]$, respectively. The phase of b_0^+/b_0^- is changed by π by changing the sign of r [see Eq. (17)]. So at $\epsilon=\epsilon_{2g\,\max}$, the choice of + or − sign makes the absolute value of the amplitude of the wave function at the film/substrate interface 1 or 0, respectively. Choosing the + sign reproduces the strong enhancement of transmission intensity near the upper band-gap edge of the substrate (X_1 point) observed for very thin (1 and 2 ML) overlayers.

The surface potential used for the calculation shown in Fig. 7 is $U_{V2}(z)$, for which the potential arises abruptly from the muffin-tin zero of the film $U_{1\,\mathrm{Re}}=13.62$ eV to $U_{V2}(0)=U_a/2=-3.0$ eV at the surface plane and increases smoothly outside the film to the vacuum level over a distance on the scale of the Thomas-Fermi screening length (0.5 Å). Changing the value of $U_{V2}(0)$ by ±3.0 eV maintains the general characteristic features of the spectra, but the agreement with experiment becomes worse. We note that the step-function limit [$L\to 0$, $U_{V2}(0)=0$] also gave worse results. Changing $U_{V2}(0)$ by more than ±3 eV produces calculated spectra quite different from the experimental curves. The surface potential barrier $U_{V1}(z, L=0.5$ Å), rounded toward both the vacuum and the film side of the surface plane, gave poor agreement with the experimental data. Thus a model with the surface plane at the last muffin-tin edge and the potential step smoothed slightly to the vacuum side gives best agreement with experiment. This result provides further evidence that the surface potential barrier should exhibit a sharp increase at the surface as suggested earlier by surface resonance studies,[12,17] field emission energy distribution results,[18] and theoretical calculation.[19]

In previous papers[2,3,8] the quantum size effect (QSE) was interpreted as an interference effect between electron waves reflected at the vacuum/film and the film/substrate interfaces. Jonker *et al.*[3] successfully ex-

plained the QSE features using a simple free-electron model. In the potential-well model employed,[3] electron reflection at the interfaces resulted from a change in potential at the interfaces (shape scattering). In the present model we have shown that the electron reflection results not only from shape scattering but also from differences in the properties of the electron scatterer arrays on either side of the vacuum/film and the film/substrate interfaces. For the system Cu/Ni(001) the latter effect is in fact dominant, as the inner potential of Cu (13.76 eV) is nearly equal to that of Ni (13.62 eV) (see Sec. III B). A model calculation which assumed that the inner potentials of Cu(001) and Ni(001) were equal gave results similar to those shown here. The electron reflectivity at the interfaces is therefore seen to be strongly dependent on the band structures of the film and the substrate.

The modes of electron transmission through the film may be classified according to the combinations of the band structures as shown in the first three columns of Table I. For the case of Cu(001) epitaxial overlayers on Ni(001), each of the first three modes shown in Table I is realized over a particular energy range: mode I for $E > 9.5$ eV (where E is the incident energy measured from the Fermi level), mode II for $7.3 < E < 9.5$ eV, and mode III for $4.8 < E < 7.3$ eV.

Thomas[2] discussed the case for which the incident electron energies are within the band gap of the substrate, i.e., mode II in Table I. In this case the incident electrons are strongly reflected at the film/substrate interface by Bragg reflection. In the absence of absorption, however, the electron reflection in this energy range is unity. A model calculation for real U_1 and U_2 indeed showed total reflection and thus no quantum size oscillations for incident energies within the band gap of the substrate.

The present calculation and a simple calculation based on the free-electron model[20] for this case (mode II) show that even though the electron reflectivity is unity, the electron numbers within the film (the integrated value of the electron density over the film) oscillate when plotted as a function of incident energy. This is due to standing-wave formation within the film at discrete energies. When electrons are absorbed from the coherent current in the film and the substrate, the coherent electron reflectivity oscillates as a function of incident energy following the oscillation of the electron number within the film, as the absorbed intensity is proportional to the electron number. From model calculations for weak and strong absorption, the following results are obtained: (1) For energies in the allowed band of the Ni substrate (thus also in the allowed band of the Cu film, i.e., mode I) the quantum size oscillations are strongest for zero absorption and decrease as absorption increases, as noted by Jonker *et al.*,[3] and (2) for energies in the band gap of the substrate, i.e., mode II, absorption in the film is necessary for the presence of QSE but degradation of the QSE features similar to (1) is found for stronger absorption. We therefore conclude that the stronger quantum size features observed experimentally for incident energies within the forbidden energy gap of the substrate and its vicinity relative to the QSE features observed over the allowed energy band of the substrate are caused not only by strong Bragg reflection at the film/substrate interface, but also by electron absorption in the film of appropriate strength.

TABLE I. Modes of electron transmission through epitaxial films.

Mode	Energy bands: Film	Energy bands: Substrate	QSE features
I	Allowed	Allowed	Weak
II	Allowed	Forbidden	Strong (assuming absorption in the film)
III	Forbidden	Forbidden	No QSE
IV	Forbidden	Allowed	QSE due to resonance tunneling

In mode III, where incident electron energies are within a band gap of both the substrate and the film, electrons are strongly reflected and no QSE features are expected. This is in agreement with the experimental results (see Figs. 2 and 3).

Mode IV is not realized for the Cu/Ni(001) system but would be realized for the Ni/Cu(001) system. We carried out the calculation for this system and found that oscillatory structure was present in the energy range corresponding to mode IV for rather thin films ($\sim$4 ML). This quantum size effect is understood as a resonance in electron tunneling through the band gap of the film.

As the quantum size effect is represented through the energy dependence of $|C|^2$ [Eq. (2)], the absorption process includes all incoherent scattering—diffuse scattering as well as inelastic scattering. For the present model, absorption in the constant potential region between ion core scatterers gave reasonable results. It is interesting to note that Andersson and Kasemo[1] have analyzed the structure in electron reflectivities from disordered overlayers assuming that incoherent scattering occurs at the plane of adatom-ion cores which are arranged randomly within the plane. In a one-dimensional model a rough surface or interface may be approximately represented by several layers of lattice planes within which ion cores are arranged randomly. In the present model, therefore, roughness of the interfaces may be treated by introducing appropriate absorption at the ion core planes near the interfaces.

The QSE features in the transmission spectra are very sensitive to film structure, since the electrons are sensitive to the overall thickness of the film as well as to the lattice spacing. In the free-electron limit relative maxima (or minima) in the transmitted current occur at energies given by[3]

$$\epsilon_n = \frac{\hbar^2}{2m}\left[\frac{n\pi}{z_0}\right]^2 - U_{1\mathrm{Re}}\ , \tag{40}$$

where $n = 1,2,\ldots$ and z_0 is the film thickness. From the above relation, a 1% change in thickness causes a peak energy shift of several tenths of an eV.

In the calculations shown in Fig. 7, the lattice spacings for the film and the substrate were chosen to be the same as the bulk values of Cu and Ni (001), respectively. Changing the lattice spacing by $\pm 5\%$, produced transmission spectra which bore no resemblance to the experimen-

tal ones even in qualitative features. The calculated results shown in Fig. 7 are reproduced only when we choose lattice spacings within $\pm 0.2\%$ of the bulk values. The agreement between the experiment and the calculation is very good overall for the various Cu coverages. It should be stressed that for the different film thicknesses all the parameters are kept the same except the number of layers, and the parameters are chosen to have well accepted values.

Close examination of Fig. 7 shows that while the agreement between the experimental and the calculated results is very good (main peak positions within 0.1 eV) for the clean Ni(001), 1- and 2-ML Cu coverages and for Cu coverages greater than 6 ML, a systematic deviation of the dominant peak position (~ 0.3 eV) is observed for Cu coverages from 3 to 6 ML. The agreement for the 1- and 2-ML spectra is less sensitive to changes of lattice spacing, probably because these spectra are strongly effected by the prominent substrate feature. The good agreement for thicker films (≥ 7 ML) shows that the lattice structure throughout the film is very close to that of bulk Cu. The deviations observed from films up to 6 ML are attributed to a distortion of the film structure from that of bulk Cu. As noted in the Introduction, the Cu film is initially pseudomorphic, so that the Cu atoms conform to the lateral periodicity of the Ni(001) substrate and are thus compressed laterally relative to bulk Cu(001).

The fit of the calculated spectra for the (3—6)-ML films could be significantly improved while maintaining the excellent agreement for the 1- and 2-ML films, but at the expense of fit for the coverages greater than 6 ML by reducing the lattice plane spacing by 1.0%. This is not an entirely satisfactory solution for the (3—6)-ML films, however, because a change of lattice spacing in plane produced by pseudomorphic growth would also alter the scattering properties (t_1 and r_1) of a plane of Cu ion cores even though the scattering properties of the individual ion cores would be uneffected. It is therefore first necessary to derive the scattering properties of the ion core planes for a new lattice spacing based on phase-shift calculations for the ion cores and calculating planer scattering matrix elements before we seek full adjustment of the atomic structural parameters for the perturbed film. The present results are very encouraging in the development of electron transmission spectroscopy as a tool to obtained electronic and structural information for epitaxial films on a crystal.

V. CONCLUSION

Low-energy-electron transmission spectra were measured for epitaxially grown Cu films on a Ni(001) substrate for coverages up to 15 ML. A model of electron transmission for an overlayered solid was developed based on one-dimensional LEED theory.[10]

We have shown that the simple transmission current measurement provides characteristic transmission spectra for discrete film thickness from 1 ML to fully developed films. Combined with simple calculation, such a measurement provides information on the substrate and the film band structure as well as information on the lattice spacings of the film and substrate in the vicinity of the interface. In particular, except for one and two monolayers the calculated spectra are quite sensitive to the film lattice parameter, and through comparison with experimental spectra it is apparently possible to distinguish pseudomorphic film structure from the normal bulk structure of the film material. For thicker films, the present method provides a unique means of investigating a fully established film/substrate interface inaccessible by other nondestructive techniques.[4] Such measurements are experimentally straightforward and may be readily applied to monitor epitaxial film growth and the wetting properties of substrates.[21]

ACKNOWLEDGMENTS

This work was supported by the National Science Foundation under Grant No. DMR-82-04662. The authors gratefully acknowledge helpful discussions with E. D. Williams, N. C. Bartelt, Q.-G. Zhu, J. Vahakangas, C.-P. S. Wang, and T. L. Einstein. Computer time was provided by the Computer Science Center of the University of Maryland. One of us (B.T.J.) was supported in part by the National Research Council.

APPENDIX

We solve the Schrödinger equation following Constantinescu and Magyari,[22]

$$-\frac{\hbar^2}{2m}\frac{d^2\psi}{dz^2}+U(z)\psi=\epsilon\psi\ , \tag{A1}$$

for the potential $U(z)=U_a+U_b/(1+e^{z/L})$. Introducing the new variable

$$y=(1+e^{z/L})^{-1}\ , \tag{A2}$$

(A1) becomes

$$y(y-1)\frac{d^2\psi}{dy^2}+(1-2y)\frac{d\psi}{dy}+\left[\frac{\eta^2}{y(1-y)}-\frac{\lambda^2}{y}\right]\psi=0\ , \tag{A3}$$

where

$$\eta^2=\frac{2m}{\hbar^2}(\epsilon-U_a-U_b)L^2=k_l^2L^2\ ,$$
$$\lambda^2=\frac{2m}{\hbar^2}(-U_b)L^2\ . \tag{A4}$$

If we introduce a new function $f(y)$ through

$$\psi=y^{\nu}(1-y)^{\mu}f(y)\ , \tag{A5}$$

and impose on ν and μ the conditions

$$\nu^2=\lambda^2-\eta^2=-\frac{2m}{\hbar^2}(\epsilon-U_a)L^2=-k_r^2L^2\ ,$$
$$\mu^2=-\eta^2=-k_l^2L^2\ , \tag{A6}$$

the following differential equation for f is obtained:

$$y(1-y)f''+[(2\nu+1)-(2\nu+2\mu+2)y]f'-(\mu+\nu)(\mu+\nu+1)f=0 . \tag{A7}$$

The two particular solutions for this equation are the hypergeometric functions

$$F(\mu+\nu,\mu+\nu+1,2\nu+1,y)$$
and
$$y^{-2\nu}F(\mu-\nu,\mu-\nu+1,-2\nu+1,y) . \tag{A8}$$

Then the solution ψ is

$$\psi=C_1y^{\nu}(1-y)^{\mu}F(\mu+\nu,\mu+\nu+1,2\nu+1,y)+C_2y^{-\nu}(1-y)^{\mu}F(\mu-\nu,\mu-\nu+1,-2\nu+1,y)$$
$$\equiv C_1\psi_1+C_2\psi_2 . \tag{A9}$$

We notice the relation

$$\psi_2(\nu,\mu,y)=\psi_1(-\nu,\mu,y) . \tag{A10}$$

Using the relation

$$F(a,b,c,y)=\frac{\Gamma(c)\Gamma(c-a-b)}{\Gamma(c-a)\Gamma(c-b)}F(a,b,a+b-c+1,1-y)$$
$$+\frac{\Gamma(c)\Gamma(a+b-c)}{\Gamma(a)\Gamma(b)}(1-y)^{c-a-b}F(c-a,c-b,c-a-b+1,1-y) , \tag{A11}$$

ψ_1 may be written

$$\psi_1=A(\nu,\mu)F(\mu+\nu,\mu+\nu+1,2\mu+1,1-y)y^{\nu}(1-y)^{\mu}+A(\nu,-\mu)F(\nu-\mu,\nu-\mu+1,-2\mu+1,1-y)y^{\nu}(1-y)^{\mu} , \tag{A12}$$

where

$$A(\nu,\mu)\equiv\frac{\Gamma(2\nu+1)\Gamma(-2\mu)}{\Gamma(\nu-\mu)\Gamma(\nu-\mu+1)}$$

and ψ_2 immediately follows from Eq. (A10).

Now we examine the behavior of the wave functions ψ_1 and ψ_2 at $z\to\pm\infty$. From Eq. (A6) we choose

$$\nu=-ik_rL \quad \text{and} \quad \mu=ik_lL . \tag{A13}$$

As $z\to+\infty$, $y\sim e^{-z/d}\to 0$, and $F(y)\to 1$. From Eq. (A9), we then have

$$\psi_1\to y^{\nu}\cong\exp(ik_rz) ,$$
$$\psi_2\to y^{-\nu}\cong\exp(-ik_rz) , \tag{A14}$$

and

$$\psi\to C_1e^{+ik_rz}+C_2e^{-ik_rz} .$$

As $z\to-\infty$, $y\to 1$, $1-y\simeq e^{z/L}\to 0$, and $F(1-y)\to 1$. So, from Eqs. (A12) and (A10),

$$\psi_1\to A(\nu,\mu)e^{ik_lz}+A(\nu,-\mu)e^{-ik_lz} ,$$
$$\psi_2\to A(-\nu,\mu)e^{ik_lz}+A(-\nu,-\mu)e^{-ik_lz} ,$$

and

$$\psi\to[C_1A(\nu,\mu)+C_2A(-\nu,\mu)]e^{ik_lz}$$
$$+[C_1A(\nu,-\mu)+C_2A(-\nu,-\mu)]e^{-ik_lz} . \tag{A15}$$

For a wave incident from left to right, now we expect $\psi(z\to\pm\infty)$ to have the forms

$$\psi(z\to-\infty)=e^{ik_lz}+r^+e^{-ik_lz} ,$$
$$\psi(z\to+\infty)=t^+e^{ik_rz} . \tag{A16}$$

Upon comparison with Eqs. (A14) and (A15) we immediately have

$$C_1A(\nu,\mu)+C_2A(-\nu,\mu)=1 ,$$
$$C_1A(\nu,-\mu)+C_2A(-\nu,-\mu)=r^+ ,$$
$$C_1=t^+ , \tag{A17}$$
$$C_2=0 .$$

Solving for t^+ and r^+ gives

$$t^+=1/A(\nu,\mu) ,$$
$$r^+=A(\nu,-\mu)/A(\nu,\mu) . \tag{A18}$$

In a similar manner, for a wave incident from right to left we expect ψ to have the forms

$$\psi(z\to+\infty)=e^{ik_rz}+r^-e^{-ik_rz} ,$$
$$\psi(z\to-\infty)=t^-e^{-ik_lz} . \tag{A19}$$

Upon comparison with Eqs. (A14) and (A15) we have

$$C_1A(\nu,\mu)+C_2A(-\nu,\mu)=0 ,$$
$$C_1A(\nu,-\mu)+C_2A(-\nu,-\mu)=t^- , \tag{A20}$$
$$C_2=1 ,$$
$$C_1=r^- .$$

Solving for t^- and r^- gives

$$r^-=-A(-\nu,\mu)/A(\nu,\mu) ,$$
$$t^-=A(-\nu,-\mu)+r^-A(\nu,-\mu) . \tag{A21}$$

*On leave from Institute of Scientific and Industrial Research, Osaka University, Ibaraki, Osaka 567, Japan.

†Present address: Naval Research Laboratory, Code 6635.J, Washington, D.C. 20375.

[1]S. Andersson and B. Kasemo, Surf. Sci. **32**, 78 (1972).

[2]R. E. Thomas, J. Appl. Phys. **41**, 5330 (1970).

[3]B. T. Jonker, N. C. Bartelt, and R. L. Park, Surf. Sci. **127**, 183 (1983).

[4]B. T. Jonker and R. L. Park, Surf. Sci. **146**, 93 (1984); **146**, 511 (1984).

[5]J. Maserjian, J. Vac. Sci. Technol. **11**, 996 (1974).

[6]R. C. Jaklevic and L. C. Davis, Phys. Rev. B **26**, 5391 (1982); R. C. Jaklevic, *ibid.* **30**, 5494 (1984).

[7]G. Bader, G. Perluzzo, L. G. Caron, and L. Sanche, Phys. Rev. B **30**, 78 (1984).

[8]B. Jonker and R. L. Park, Solid State Commun. **51**, 871 (1984).

[9]A. Chambers and D. C. Jackson, Philos. Mag. **31**, 1357 (1975).

[10]J. B. Pendry, *Low-Energy Electron Diffraction* (Academic, London, 1974), pp. 84ff.

[11]N. W. Ashcroft and N. D. Mermin, *Solid State Physics* (Holt, Rinehart and Winston, New York, 1975).

[12]R. E. Dietz, E. G. McRae, and R. L. Campbell, Phys. Rev. Lett. **45**, 1280 (1980).

[13]F. Szmulowicz and D. M. Pease, Phys. Rev. B **17**, 3341 (1978).

[14]G. A. Burdick, Phys. Rev. **129**, 138 (1963).

[15]S. Andersson, Surf. Sci. **18**, 325 (1969).

[16]R. Lässer, N. V. Smith, and R. L. Benbow, Phys. Rev. B **24**, 1895 (1981).

[17]J. M. Baribeau and J. D. Carette, Surf. Sci. **112**, 241 (1981).

[18]A. Modinos and G. Oxinos, J. Phys. C **14**, 1373 (1981).

[19]J. C. Inkson, Surf. Sci. **28**, 69 (1971).

[20]Ref. 11, p. 369.

[21]G. Perluzzo, L. Sanche, C. Gaubert, and R. Baudoing, Phys. Rev. **B30**, 4292 (1984).

[22]F. Constantinescu and E. Magyari, *Problems in Quantum Mechanics* (Pergamon, New York, 1971).